

# A New Characterization of Fine Scale Diffusion on the Cell Membrane \*

Flor A. Espinoza

Department of Mathematics and Statistics

Kennesaw State University

Atlanta, GA 30144-5591 USA

Stanly L. Steinberg<sup>†</sup>

The Center for the Spatiotemporal Modeling of Cell Signaling

Department of Mathematics and Statistics

University of New Mexico

Albuquerque NM 87131-1141 USA

June 17, 2021

---

\*This work was supported in part by NIH grant P50 GM085273, supporting the Center for Spatiotemporal Modeling of Cell Signaling, and by NIH grants R01 GM49814 and R01 AI051575.

# Contents

<b>1</b>	<b>Introduction</b>	<b>4</b>
1.1	Random Variables . . . . .	5
1.2	Tracking Data . . . . .	6
<b>2</b>	<b>Analyzing the Data</b>	<b>7</b>
2.1	Scaling the Data . . . . .	8
<b>3</b>	<b>Fitting the Data</b>	<b>10</b>
3.1	The double power law distribution . . . . .	10
3.2	Simulating the double power law distribution . . . . .	11
3.3	Fitting the PDF and CDF . . . . .	12
<b>4</b>	<b>Results and Discussion</b>	<b>14</b>
<b>A</b>	<b>The fits of the CDFs and PDFs</b>	<b>18</b>

## List of Tables

1.1	The total number of jumps for 1, 2, and 3 time steps that are in data sets $A$ and $B$ . . . . .	6
3.1	The values $\alpha$ , $\beta$ , $s$ and the residual for the fits. . . . .	12

## List of Figures

2.1	The CDFs for data sets A and B . . . . .	7
2.2	The PDFs for data sets A and B . . . . .	7
2.3	The scaled CDFs for all data in the data sets A and B . . . . .	8
2.4	The scaled PDFs for all data in the data sets A and B . . . . .	8
3.1	The analytic and simulated $pl$ and $PL$ distributions with $\sigma = 1$ are essentially identical. . . . .	11
3.2	Plots of the fits of both the PDF and CDF of the data. The vertical red line indicates the cut off used for fitting the data. . . . .	12
A.1	The PDFs fits for data sets A and B and 1, 2, and 3 jumps. . . . .	18

## Abstract

We use a large single particle tracking data set to analyze the short time and small spatial scale motion of quantum dots labeling proteins in cell membranes. Our analysis focuses on the jumps which are the changes in the position of the quantum dots between frames in a movie of their motion. Previously we have shown that the directions of the jumps are uniformly distributed and the jump lengths can be characterized by a double power law distribution.

Here we show that the jumps over a small number of time steps can be described by scalings of a *single* double power law distribution. This provides additional strong evidence that the double power law provides an accurate description of the fine scale motion. This more extensive analysis provides strong evidence that the double power law is a novel stable distribution for the motion. This analysis provides strong evidence that an earlier result that the motion can be modeled as diffusion in a space of fractional dimension roughly  $3/2$  is correct. The form of the power law distribution quantifies the excess of short jumps in the data and provides an accurate characterization of the fine scale diffusion and, in fact, this distribution gives an accurate description of the jump lengths up to a few hundred nanometers. Our results complement of the usual mean squared displacement analysis used to study diffusion at larger scales where the proteins are more likely to strongly interact with larger membrane structures.

KeyWords: Single particle tracking, Protein motion, Jump probability distribution, Stable distribution,

# 1 Introduction

Our goal is to better understand the fine scale motion of proteins in cell membranes. We do this by studying a large single particle tracking data set for the *IgE* high affinity receptor *FcεRI* tagged with quantum dots (QDs) [10, 27] which were taken from movies of the positions of the QDs. Standard time series analysis requires the analysis of the jumps which are the changes in the positions of the QDs between frames in the movie as was done in [10, 27]. The components of the jumps in a Brownian random walk in two dimensions are normally distributed if and only if the directions of the jumps are uniformly distributed and the lengths of the jumps have a chi, or equivalently, Weibull distribution. A main result of the previous studies is that the directions of the jumps are uniformly distributed, just as in Brownian motion, but the jump lengths do not have a chi distribution. Instead the studies provide evidence that the jumps can be described using a double power law distribution. It was also shown in [10], that a double power law fits the jump data better than general chi or general Weibull distributions. Our power law distribution has two power law behaviors, most importantly one for small jumps and another less important power law behavior for large jumps.

Here we study the jumps over a few time steps, not just one time step, and provide much stronger evidence that the previous descriptions of the motion are accurate. It came as a surprise to us that the double power laws for multiple time steps are related to the one time step power law by a square root of time scaling law, just as in Brownian motion. This allows us to characterize the diffusion on short time and small spatial scales using a single double power law probability distribution function with scaling and is the key to providing stronger evidence for the previous characterization of the motion. Actually the double power law is surprisingly accurate for moderate spatial and temporal scales, does not have a heavy tail [8, 17] and, in fact, has many finite moments.

An important point is that the measured motion of the quantum dots has several components one of which is the actual motion of the protein. These include movement of the dot while the image is being taken, noise in the imaging equipment, and the super resolution imaging process. These errors have been studied extensively in the context of MSD analysis, see e.g. [4, 9, 11, 15, 16, 18, 21, 23, 24]. However, it is reasonable to assume that all these random processes are independent, and all but the underlying motion of the protein are normally distributed. If the underlying motion of the protein was normally distributed, then the measured motion would also be normally distributed, but it is not. The most likely and cause of the double power law behavior is the motion of the proteins.

This work has important implications for modeling protein motion. The Central Limit Theorem implies that if we could model our data as an random walk in a homogeneous medium that has independent and identically distributed (IID) jumps with double power law distributed jump lengths, then the components of the jumps over many time steps should approach a normal distribution, or equivalently, the jump angles must be uniformly distributed and the jump lengths must have a chi distribution. We can view our data as sampling the motion after the protein has made many smaller time steps. If the motion

could be described as an IID random walk then jump lengths must have a chi distribution, which they do not have. We view this to mean that the diffusion of proteins in the cell membrane is a complex process that cannot be accurately modeled using an IID random walk in a homogeneous medium. We note that previous work [10] supports the assumption that the jumps are independent. Collaborators have recently made simulations of random walks in non-homogeneous mediums that have statistics similar to our data [7].

To understand why we view the motion as diffusion in a space of dimension  $3/2$ , one needs to know that in dimension  $n$ , IID random walks where the components of the motion are normally distributed with mean zero and standard deviation  $\sigma$ , the motion can also be characterized as uniform on the unit sphere and radially by the chi distribution with  $n$  degrees of freedom and scale factor  $s$ ,  $c(r, s, n) = c(r/s, n)/s$  where [10]

$$c(r, n) = \frac{2}{2^{n/2}\Gamma(n/2)} r^{n-1} e^{-\frac{r^2}{2}}, \quad (1.1)$$

$r \geq 0$ ,  $n s^2 = \sigma^2 > 0$  and  $n \geq 1$ . In two dimensions this is known as the chi or Weibull distribution while in dimension three it is the Maxwell-Boltzmann distribution. For small  $r$ , this distribution has the form

$$c(r, n) \approx C r^{n-1},$$

where  $C$  is a constant. Consequently, for the fine scale motion, if a probability distribution function for the lengths of jumps has the form

$$p(r) \approx C r^{d-1},$$

for small  $r$  and where  $C$  is a constant, then we say that the motion can be modeled as being in a space of dimension  $d$ . For our data,  $d \approx 3/2$ . This is a quantitative measure of the restrictions on the motion of the protein on small spatial and temporal scales.

Our results complement those obtained by mean squared displacement analysis which involves using data from more time steps than used here and consequently are appropriate to temporal and spatial scales where the proteins may have strong interactions with other membrane structures [1, 5, 6, 12, 13, 20, 22, 26].

The biology and microscopy involved in creating the data are described in detail in [2, 3], so we will not repeat this here. We will use the same notation as in [10], which we now summarize.

## 1.1 Random Variables

We model the QDs positions using vector valued random variables:

$$\vec{\mathbf{P}}_n = (\mathbf{X}_n, \mathbf{Y}_n), \quad 1 \leq n \leq N, \quad N > 0,$$

where  $\mathbf{X}_n$  and  $\mathbf{Y}_n$  are real valued random variables and  $N$  and  $n$  are integers. The jumps are also random variables:

$$\vec{\mathbf{J}}_n = \vec{\mathbf{P}}_n - \vec{\mathbf{P}}_{n-1} = (\Delta\mathbf{X}_n, \Delta\mathbf{Y}_n), \quad 2 \leq n \leq N.$$

	$k = 1$	$k = 2$	$k = 3$
$A$	407,669	346,750	302,256
$B$	353,368	300,517	261,474

Table 1.1: The total number of jumps for 1, 2, and 3 time steps that are in data sets  $A$  and  $B$ .

In polar coordinates, the lengths of the jumps  $\mathbf{L}_n$  and the angles  $\Theta_n$  between the jump vectors and the  $x$ -axis are also real valued random variables:

$$\mathbf{L}_n = \|\vec{\mathbf{J}}_n\| = \sqrt{\Delta\mathbf{X}_n^2 + \Delta\mathbf{Y}_n^2}, \quad \Theta_n = \arctan(\Delta\mathbf{Y}_n, \Delta\mathbf{X}_n), \quad 2 \leq n \leq N,$$

where  $\arctan$  gives a value in  $(-\pi, \pi]$  such that if  $\mathbf{L}_n \neq 0$ , then  $\cos(\Theta_n) = \Delta\mathbf{X}_n/\mathbf{L}_n$  and  $\sin(\Theta_n) = \Delta\mathbf{Y}_n/\mathbf{L}_n$ , and consequently,  $\tan(\Theta_n) = \Delta\mathbf{Y}_n/\Delta\mathbf{X}_n$  if  $\Delta\mathbf{X}_n \neq 0$ . If  $\vec{\mathbf{J}} = (0, 0)$ , then  $\Theta = 0$  (in matlab).

## 1.2 Tracking Data

The analyzed data were taken from unstimulated cells where a subset of the FceRI on the cell membrane were labeled with QDs. We studied two large data sets called  $A$  and  $B$ . We analyzed each data set individually as it is useful to see the differences between the two sets but for our new results we combine the data sets to obtain better accuracy. The data contain  $M > 0$  tracks with  $N > 0$  positions described by

$$x_{m,n}, \quad y_{m,n}, \quad v_{m,n}, \quad 1 \leq m \leq M, \quad 1 \leq n \leq N.$$

The vectors

$$\vec{r}_{m,n} = (x_{m,n}, y_{m,n})$$

estimate the position of the QDs. If  $v_{m,n} = 1$ , then the QD is on and the position of the QD is valid data, while if  $v_{m,n} = 0$ , the QD is off.

The length of a valid jump of over  $k$  times steps is

$$L_{m,n,k} = \|\vec{r}_{m,n+k} - \vec{r}_{m,n}\|, \quad 1 \leq m \leq M, \quad 1 \leq n \leq N - k.$$

The jump is valid provided that the QD is on at all times  $n$  through  $n + k$ , that is

$$v_{m,n} * v_{m,n+1} * \dots * v_{m,n+k} = 1, \quad 1 \leq m \leq M, \quad 1 \leq n \leq N - k.$$

The number of valid jumps in data sets  $A$  and  $B$  is given in Table 1.1. These are large data sets.

## 2 Analyzing the Data

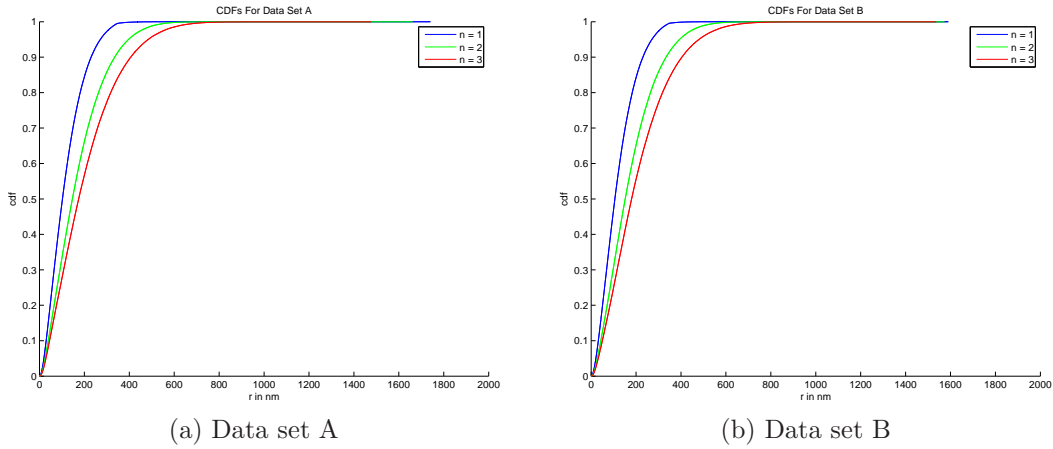


Figure 2.1: The CDFs for data sets A and B

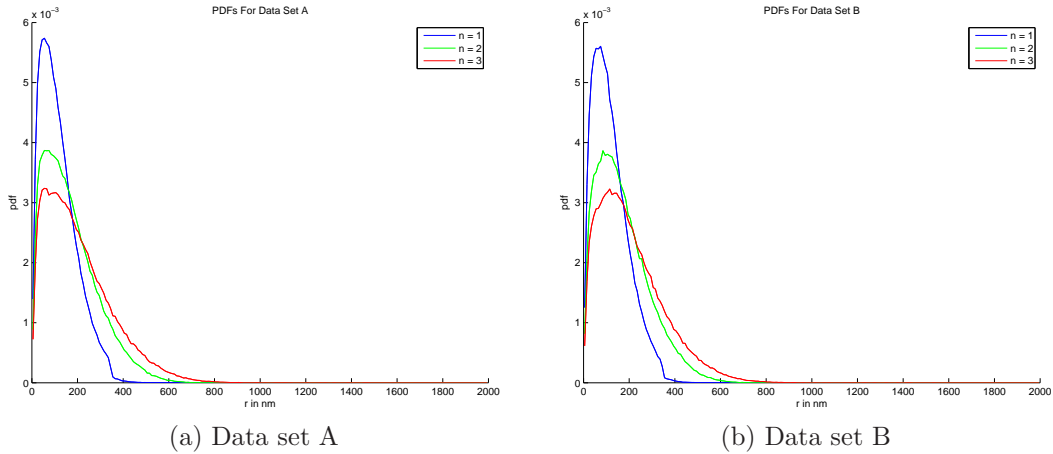


Figure 2.2: The PDFs for data sets A and B

Our first step in analyzing the data is to plot the cumulative distribution functions (CDFs) and probability distribution functions (PDFs) of the jump lengths which are shown in Figures 2.1 and 2.2. The CDF is computed by first sorting the lengths into increasing size. Assuming that there are  $I > 0$  lengths  $r_i$ ,  $1 \leq i \leq I$  then increasing size means that  $r_i \leq r_{i+1}$ ,  $1 \leq i \leq I-1$ . The CDFs shown in Figure 2.1 are determined by the pairs  $(r_i, i/I)$ . This method of determining the CDFs is helpful as it makes use of all of the data without any averaging like that which occurs when binning the data. Next we find the PDFs shown in Figure 2.2 by the standard method of binning the data using 200 bins, thus averaging over about 1/2% of the data for each value of the PDF. These plots use all of the valid jumps

in each of the data sets and  $n$  is the number of time steps determining the jumps. Observe that as the number of time steps increase, the height of the PDFs decreases while the width increases, suggesting that the PDFs are related by a scaling. As can be seen in Figure 2.2 and noted in [10], for the single time step jumps ( $n = 1$ ), the data for  $r > 346\text{nm}$  have significant errors and consequently are not used in our analysis. As we are most interested in short jumps, this does not cause a problem.

## 2.1 Scaling the Data

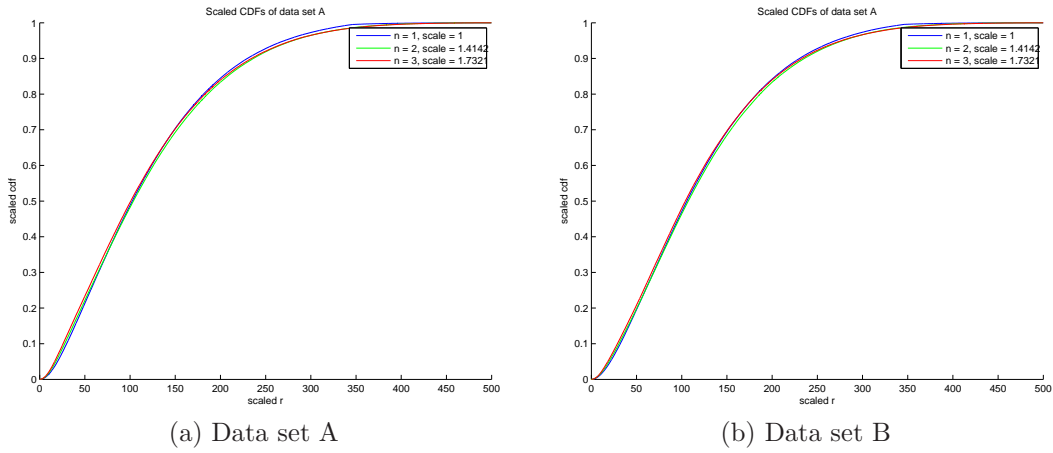


Figure 2.3: The scaled CDFs for all data in the data sets A and B

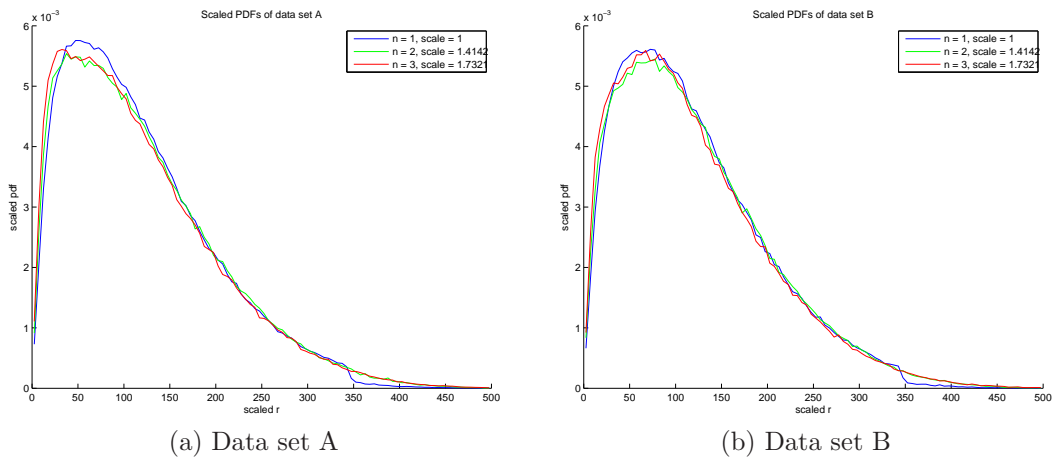


Figure 2.4: The scaled PDFs for all data in the data sets A and B



If the CDF and PDF are smooth then they are related by

$$p(r) = \frac{dP(r)}{dr}.$$

If  $s > 0$  is to be used as a scaling factor, then the scaled CDF and PDF are given by

$$P\left(\frac{r}{s}\right) \text{ and } \frac{1}{s}p\left(\frac{r}{s}\right).$$

We tried scaling the data for 1, 2 and 3 time step jumps by  $\sqrt{1} = 1$ ,  $\sqrt{2}$  and  $\sqrt{3}$  which is done by dividing the jumps by the scale factor. The results of the scaling are shown in Figures 2.3 and 2.4. It is a surprise that the scaled CDFs and PDFs are so similar and the scaling property is the same as for Brownian motion. Thus, even though the components of the jumps are not normally distributed, the angles of the jumps can be modeled as uniformly distributed and the jump lengths can be modeled by a single PDF or CDF that is scaled by  $\sqrt{t}$ . We now turn to quantifying this idea.

Because of the errors in the single time step jumps for for  $r > 346\text{nm}$  we only analyze the scaled data for  $r \leq 346\text{nm}$  which corresponds to the unscaled jumps satisfying  $r \leq 346\text{nm}$  when  $n = 1$ ,  $r \leq 489\text{nm}$  when  $n = 2$  and  $r \leq 599\text{nm}$  when  $n = 3$ . However, we plot our results for scaled data satisfying  $r \leq 500\text{nm}$  which scales to  $r \leq 500\text{nm}$  when  $n = 1$ ,  $r \leq 707\text{nm}$  when  $n = 2$  and  $r \leq 866\text{nm}$  when  $n = 3$  to emphasize that are results are quite good even for large jumps

### 3 Fitting the Data

We begin by describing the double power law distribution and its scaling law. We then show how to generate random numbers having the double power law probability distribution function and finish by using the double power law to fit the jump data.

#### 3.1 The double power law distribution

In order for the parameters to have a more intuitive meaning we will change the notation from that in [10]. The functional form is chosen in a way that the PDF  $p(r)$  is a power law for both small and large  $r$ , which is substantially more restrictive than having only one of these conditions hold. Additionally, we required that the PDF has a simple CDF so that it is easy to simulate random numbers with the given PDF. The result is our *double power law*.

For small  $r \geq 0$ , we require

$$p(r) \approx C_1 r^{\alpha-1}, \quad \alpha \geq 1,$$

because then  $\alpha$  corresponds to the dimension of the space (see (1.1)) in which the diffusion is occurring. For large  $r$  we want the PDF to decay rapidly, so we choose

$$p(r) \approx \frac{C_2}{r^\beta}, \quad \beta > 1.$$

The condition on  $\beta$  guarantees that the PDF has a finite integral. We find a good choice for the PDF  $p$  and corresponding CDF  $P$  is

$$P(r) = 1 - \frac{1}{(1+r^\alpha)^{(\beta-1)/\alpha}}, \quad p(r) = \frac{(\beta-1)r^{\alpha-1}}{(1+r^\alpha)^{(\alpha-1+\beta)/\alpha}}, \quad r \geq 0.$$

Also, to make the values of the parameters easy to interpret, we need to find a scale factor  $S$  so that the second moment of the scaled power law will be one. The first and second moments of any distribution  $p$  are:

$$m_1 = \int_0^\infty r p(r) dr, \quad m_2 = \int_0^\infty r^2 p(r) dr.$$

For the power law distribution, integration gives

$$m_1 = \frac{\Gamma\left(\frac{\alpha+1}{\alpha}\right) \Gamma\left(\frac{\beta-2}{\alpha}\right)}{\Gamma\left(\frac{\beta-1}{\alpha}\right)}, \quad m_2 = \frac{\Gamma\left(\frac{\alpha+2}{\alpha}\right) \Gamma\left(\frac{\beta-3}{\alpha}\right)}{\Gamma\left(\frac{\beta-1}{\alpha}\right)}.$$

If we set

$$pl(r) = S p(Sr), \quad PL(r) = P(Sr), \tag{3.1}$$

then

$$\int_0^\infty pl(r) dr = 1,$$

and the first and second moments of this distribution are

$$M_1 = \frac{m_1}{S}, \quad M_2 = \frac{m_2}{S^2}.$$

Consequently, if

$$S = \sqrt{m_2}, \tag{3.2}$$

then

$$M_2 = 1.$$

The required double power law distributions are then given by (3.1).

### 3.2 Simulating the double power law distribution

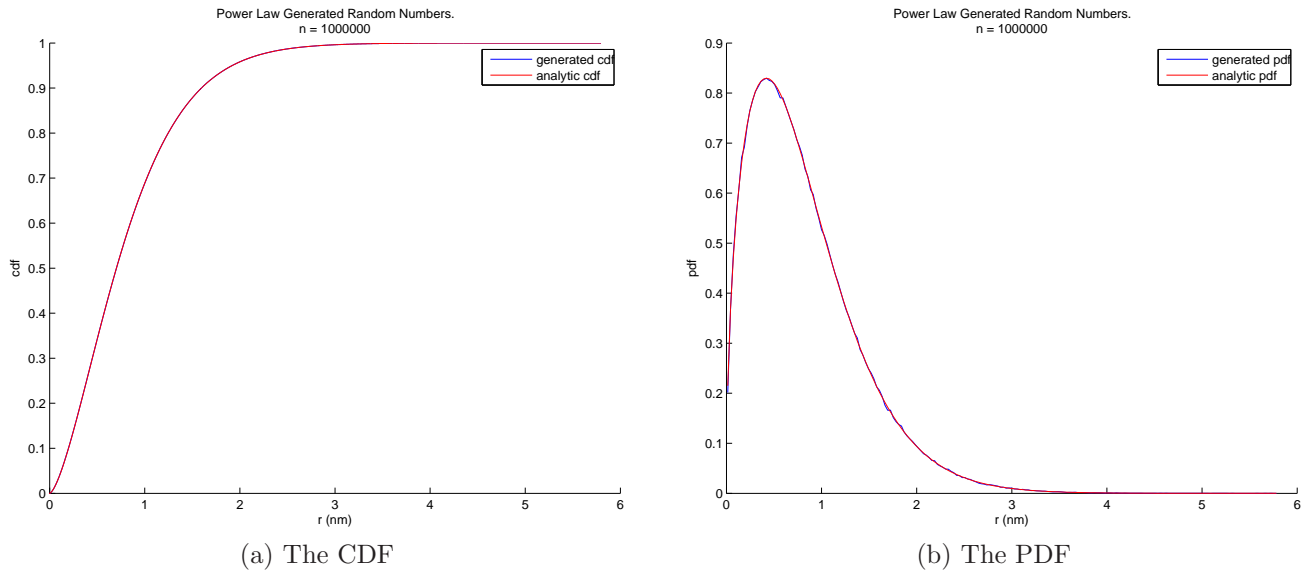


Figure 3.1: The analytic and simulated  $pl$  and  $PL$  distributions with  $\sigma = 1$  are essentially identical.

As is well known, if  $r$  is a uniformly distributed random number in  $[0, 1]$ , then solving  $P(r) = u$  will produce random number with the given CDF  $P$  and associated PDF  $p$ . Therefore, we can generate random number with the  $pl$  distribution by solving

$$PL(r) = u$$

where  $u$  is uniformly distributed. This gives

$$r = \frac{1}{S} \left( -1 + (1 - u)^{-\alpha/(-1+\beta)} \right)^{1/\alpha},$$

	$\alpha$	$\beta$	$s(\text{nm})$	residual
PDF	1.49	39.47	148.52	1.9e-08
CDF	1.49	256.86	145.73	6.8e-06

Table 3.1: The values  $\alpha$ ,  $\beta$ ,  $s$  and the residual for the fits.

where  $S$  is given in (3.2). Because  $u$  is a uniformly distributed random number in  $[0, 1]$ , then so in  $1 - u$  so this can be simplified to

$$r = \frac{1}{S} \left( -1 + u^{-\alpha/(-1+\beta)} \right)^{1/\alpha} .$$

We numerically checked that this distribution has  $\sigma = 1$  and plot the comparisons of the simulated and analytic PDF and CDF in Figure 3.1. Double power law random numbers with second moment  $\sigma^2$  are given by  $\sigma r$ .

### 3.3 Fitting the PDF and CDF

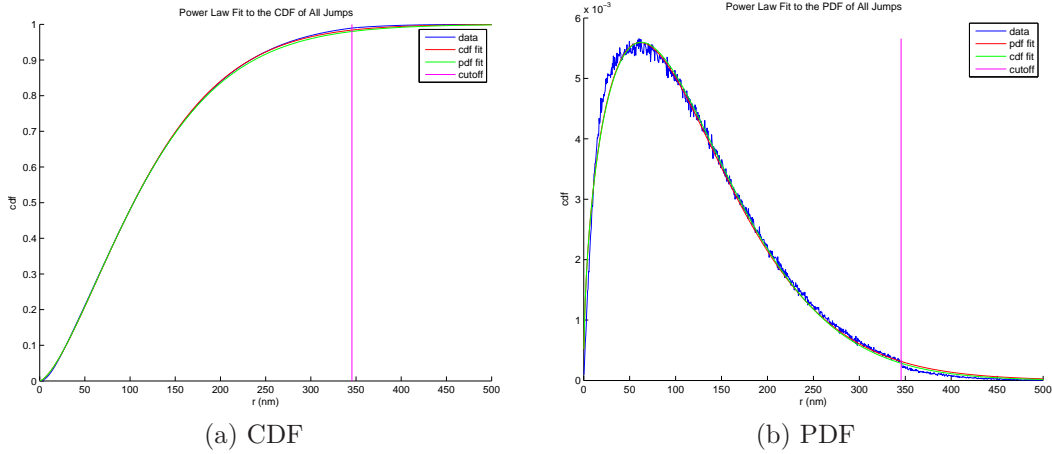


Figure 3.2: Plots of the fits of both the PDF and CDF of the data. The vertical red line indicates the cut off used for fitting the data.

We now use least-squares data fitting to find a double exponential power law that fits the jump data, that is, we must estimate the parameters  $\alpha$  and  $\beta$  and the scale parameter  $s$ . To obtain maximal accuracy for the parameters, we combine all the scaled jumps sizes from data sets  $A$  and  $B$  and scaled jumps sizes for 1, 2 and 3 time steps. As noted above, and can be seen in Figure 3.2b, the data for  $r > 346\text{nm}$  have significant errors, so we only fit jumps for  $r \leq 346\text{nm}$  which gives 1,971,537 values that can be used for the fits, which are excellent for  $r \leq 346\text{nm}$ .

In fact, we fit both the PDF and CDF independently to obtain

$$\begin{aligned} &\alpha_{\text{CDF}}, \quad \beta_{\text{CDF}}, \quad s_{\text{CDF}}, \\ &\alpha_{\text{PDF}}, \quad \beta_{\text{PDF}}, \quad s_{\text{PDF}}. \end{aligned}$$

But the parameters of the fit of the PDF can be used in the fit to the CDF and conversely. As is common with fitting problems, the solution is not unique, as shown in Table 3.1, but the graphs of the fits are essentially the same. We consider the fit with  $\beta \approx 40$  the simplest and thus the better fit. We plot both of these fits in Figure 3.2. We are most interested in the parameter  $\alpha$  which describes the short jumps and is *unique*. Also, the square root of the second moment of all of the scaled jumps is 143.85nm and indeed the scale factors, as expected, are close to this value.

## 4 Results and Discussion

We have shown that the small spatial and short time motion of QDs labeling proteins on the cell membrane can be characterized by a single double power law and square root of time scaling. In fact, this distribution is a good fit for all of the scaled jumps under 340nm. This power law quantifies the idea that this motion has substantially more short jumps than if the motion was a Brownian random walk. Another way to say this is that the motion can be viewed as diffusion in a space of dimension  $3/2$ , which also quantifies the small scale restrictions of the motion. We note that this notion of diffusion seems not to be closely related to diffusion on fractals [19] where the MSD was used to characterize the motion. On the other hand, the fact that the jumps over a few time steps are all described by one probability distribution and a scale factor suggests that this distribution is *stable* [17] and thus captures important properties of the motion.

To accurately study the interaction of molecules on a cell membrane one can use a stochastic simulator where the time step is chosen so the the proteins typically move only a few nanometers. Our results can be extend to provide the probability that two proteins will interact in time intervals where the proteins move a few hundred nanometers, providing a tool for significantly reducing the simulation cost.

We note that the Central Limit Theorem puts a strong restrictions on modeling the motion. To confirm this, we used our double power law random number generator combined with uniformly generated angles to simulate random walks. For a 100 walkers going 10 time steps, the distribution of the distance moved over the 10 steps is now normally distributed as predicted by the Central Limit Theorem. This implies that the motion cannot be accurately modeled as a IID random walk in a homogeneous medium.

Researchers associated with the New Mexico Center for the Spatiotemporal Modeling of Cell Signaling have created models of the cell membrane that include models of actin filament barriers and lipid rafts where the jump data has properties similar to the jump data analyzed here. It is hoped that these models will provide a connection between the statistics of the membrane structure and the resulting PDF of the jump sizes.

Our results complement recent results on the analysis of the motion of proteins on longer time scales using mean squared displacement ideas. For example: [4] uses k-space image correlation spectroscopy analysis to study single molecule density data of lipids and proteins labeled with quantum dots; [18] uses variational Bayesian treatment of hidden Markov models to analyze many short tracks identifying several diffusion states; [14] uses nonergodic motion, fractal structures, and multifractional random motion to study the motion of proteins; [15] uses Bayesian statistics to better quantify noise from sampling limitations and biological heterogeneity; [25] shows that both ergodic and a nonergodic process exist in the plasma membrane and that the ergodic process resembles a fractal structure originating in the macromolecular crowding in the cell membrane; [9] uses hidden Markov models are used to identify multiple states of diffusion within experimental trajectories.

## References

- [1] D. Alcor, G. Gouzer, and A. Triller. Single-particle tracking methods for the study of membrane receptors dynamics. *EUR J NEUROSC*, 30(6):987–997, 2009.
- [2] N. L. Andrews, K. A. Lidke, J. R. Pfeiffer, A. R. Burns, B. S. Wilson, and J. M. Oliver. Actin restricts Fc $\epsilon$ RI diffusion and facilitates antigen induced receptor immobilization. *NAT CELL BIOL*, 10(8):955–962, 2008.
- [3] N. L. Andrews, J. R. Pfeiffer, A. M. Martinez, D. M. Haaland, R. W. Davis, T. Kawakami, J. M. Oliver, B. S. Wilson, and D. S. Lidke. Small, mobile Fc $\epsilon$ RI aggregates are signaling competent. *Immunity*, 31(3):469–479, 2009.
- [4] E. C. Arnspang, J. Schwartzentruber, M. P. Clausen, P. W. Wiseman, and B. C. Lagerholm. Bridging the gap between single molecule and ensemble methods for measuring lateral dynamics in the plasma membrane. *PLoS ONE*, 8(12), 2013.
- [5] K. Baba and K. Nishida. Single-molecule tracking in living cells using single quantum dot applications. *Theranostics*, 2(7):655–667, 2012.
- [6] J. C. Chang and S. J. Rosenthal. Real-time quantum dot tracking of single proteins. In Sarah J. Hurst, editor, *Biomedical Nanotechnology*, volume 726 of *Methods in Molecular Biology*, pages 51–62. Humana Press, 2011.
- [7] Y. Chen, C. Short, .M. Halász, and J.S. Edwards. The impact of high density receptor clusters on vegf signaling. In *Electronic Proceedings in Theoretical Computer Science*, volume 125, pages 37–52. Second International Workshop on Hybrid Systems and Biology (HSB 2013), 9 2013.
- [8] A. Clauset, C. Shalizi, and M. Newman. Power-law distributions in empirical data. *SIAM REV*, 51(4):661–703, 2009.
- [9] R. Das, C. W. Cairo, and D. Coombs. A hidden markov model for single particle tracks quantifies dynamic interactions between lfa-1 and the actin cytoskeleton. *PLoS COMPUT BIOL*, 5(11), 2009.
- [10] F. A. Espinoza, M. J. Wester, J. M. Oliver, B. S. Wilson, N. L. Andrews, D. S. Lidke, and S. L. Steinberg. Insights into cell membrane microdomain organization from live cell single particle tracking of the ige high affinity receptor Fc $\epsilon$ RI of mast cells. *B MATH BIOL*, 74(8):1857–1911, 2012.
- [11] E. Kepten, I. Bronshtein, and Y. Garini. Improved estimation of anomalous diffusion exponents in single-particle tracking experiments. *PHYS REV E*, 87:052713, May 2013.

- [12] D. S. Lidke, S. T. Low-Nam, P. J. Cutler, and K. A. Lidke. Determining FcεRI diffusional dynamics via single quantum dot tracking. In J.P. Rast and J.W.D. Booth, editors, *Immune Receptors*, volume 748 of *Methods in Molecular Biology*, pages 121–132. Humana Press, 2011.
- [13] S. Manley, J. M. Gillette, and J. Lippincott-Schwartz. Chapter five - single-particle tracking photoactivated localization microscopy for mapping single-molecule dynamics. In Nils G. Walter, editor, *Single Molecule Tools, Part B: Super-Resolution, Particle Tracking, Multiparameter, and Force Based Methods*, volume 475 of *Methods in Enzymology*, pages 109 – 120. Academic Press, 2010.
- [14] T. T. Marquez-Lago, A. Leier, and K. Burrage. Anomalous diffusion and multifractional brownian motion: simulating molecular crowding and physical obstacles in systems biology. *IET SYST BIOL*, 6(4):134 – 142, 2012.
- [15] N. Monnier, S.-M. Guo, M. Mori, J. He, P. Lénárt, and M. Bathe. Bayesian approach to msd-based analysis of particle motion in live cells. *BIOPHYS J*, 103(3):616–626, 04 2012.
- [16] A. Nandi, D. Heinrich, and B. Lindner. Distributions of diffusion measures from a local mean-square displacement analysis. *PHYS REV E*, 86:021926, Aug 2012.
- [17] J. P. Nolan. *Stable Distributions - Models for Heavy Tailed Data*. Birkhauser, Boston, 2013. In progress, Chapter 1 online at [academic2.american.edu/~jpnolan](http://academic2.american.edu/~jpnolan).
- [18] F. Persson, M. Linden, C. Unoson, and J. Elf. Extracting intracellular diffusive states and transition rates from single-molecule tracking data. *NAT METHODS*, 10(3):265–269, Mar 2013.
- [19] J. Prehl. *Diffusion on fractals and space-fractional diffusion equations*. PhD thesis, Technische Universit at Chemnitz, Chemnitz, Germany, 2010.
- [20] V. Rajani, G. Carrero, D. E. Golan, G. de Vries, and C. W. Cairo. Analysis of molecular diffusion by first-passage time variance identifies the size of confinement zones. *BIOPHYS J*, 100(6):1463 – 1472, 2011.
- [21] T Savin and P. S. Doyle. Static and dynamic errors in particle tracking microrheology. *BIOPHYS J*, 88(1):623–638, 04 2014.
- [22] M. J. Saxton. Single-particle tracking: connecting the dots. *NAT METHODS*, 5(8):671–672, Aug 2008.
- [23] B. Shuang, C. P. Byers, L. Kisley, L.-Y. Wang, J. Zhao, H. Morimura, S. Link, and C. F. Landes. Improved analysis for determining diffusion coefficients from short, single-molecule trajectories with photoblinking. *Langmuir*, 29(1):228–234, 2013.



- [24] S. C. Weber, M. A. Thompson, W. E. Moerner, A. J. Spakowitz, and J. A. Theriot. Analytical tools to distinguish the effects of localization error, confinement, and medium elasticity on the velocity autocorrelation function. *BIOPHYS J*, 102(11):2443 – 2450, 2012.
- [25] A. V. Weigel, B. Simon, M. M. Tamkun, and D. Krapf. Ergodic and nonergodic processes coexist in the plasma membrane as observed by single-molecule tracking. *P NATL ACAD SCI USA*, 108(16):6438–6443, 2011.
- [26] Nathan P. Wells, G. A. Lessard, P. M. Goodwin, M. E. Phipps, P. J. Cutler, D. S. Lidke, B. S. Wilson, and J. H. Werner. Time-resolved three-dimensional molecular tracking in live cells. *NANO LET*, 10(11):4732–4737, 2010.
- [27] W. Ying, G. Huerta, M. Zúñiga, and Stanly Steinberg. Time series analysis of particle tracking data for molecular motion on the cell membrane. *B MATH BIOL*, 71(8):1967–2024, 2009.

# A The fits of the CDFs and PDFs

In this section we show how well the computed PDF power laws fit the unscaled data for 1, 2 and 3 jumps and data sets *A* and *B*. Again we see that the fits are excellent, but now the noise in the data is more apparent.

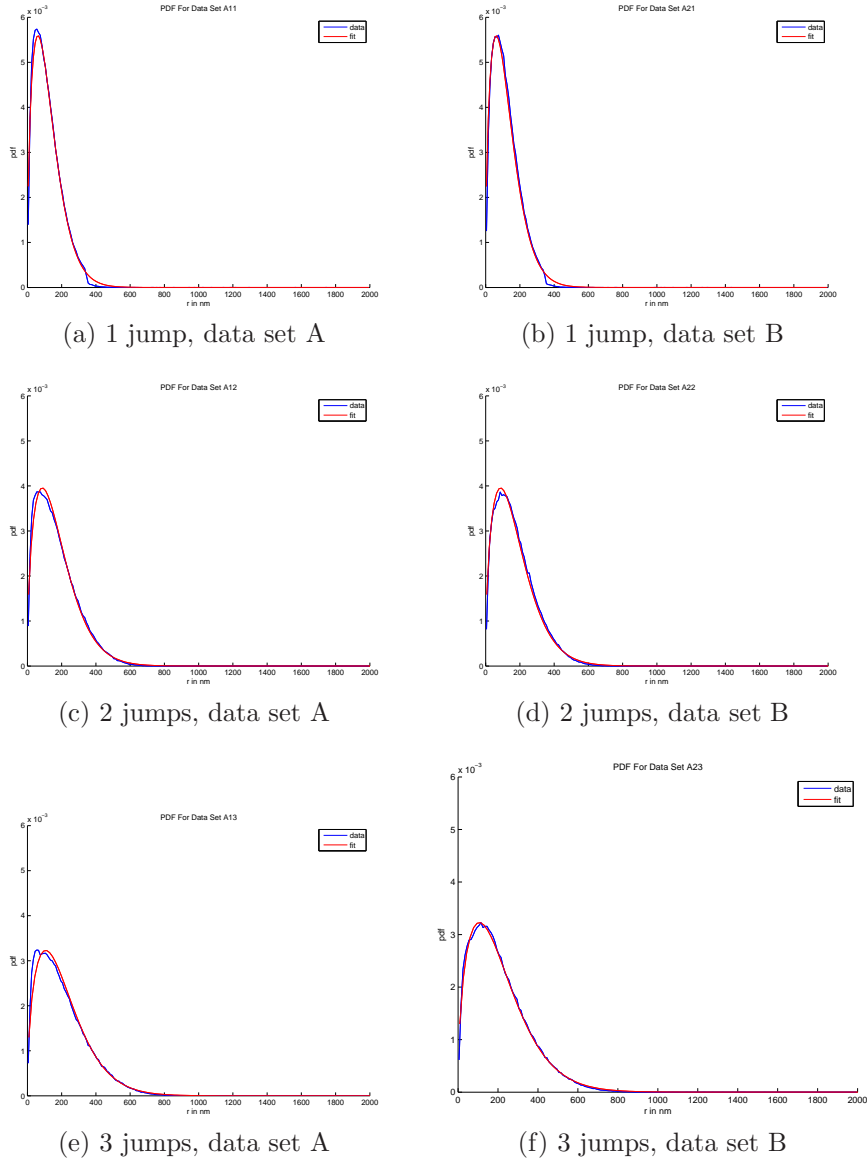


Figure A.1: The PDFs fits for data sets A and B and 1, 2, and 3 jumps.